nature chemical biology

SUPPLEMENTARY INFORMATION

https://doi.org/10.1038/s41589-019-0342-2

In the format provided by the authors and unedited.

CRISPR-Cas9 screens identify regulators of antibody–drug conjugate toxicity

C. Kimberly Tsui[1], Robyn M. Barfield[2], Curt R. Fischer[3], David W. Morgens[1], Amy Li[1], Benjamin A. H. Smith[3,4], Melissa Anne Gray[3,5], Carolyn R. Bertozzi[3,5,6], David Rabuka[2] and Michael C. Bassik[1,3]*

[1]Department of Genetics, Stanford University School of Medicine, Stanford, CA, USA. [2]Catalent Biologics, Emeryville, CA, USA. [3]Stanford ChEM-H, Stanford University, Stanford, CA, USA. [4]Department of Chemical and Systems Biology, Stanford University School of Medicine, Stanford, CA, USA. [5]Department of Chemistry, Stanford University, Stanford, CA, USA. [6]Howard Hughes Medical Institute, Stanford University, Stanford, CA, USA.
*e-mail: bassik@stanford.edu

Supplementary Information

Supplementary table 1: Sequences of sgRNAs used in this study

Sequences of sgRNA transduced into Ramos cells for individual validation	
Gene	**5' to 3' sequences**
CD22	CCTCATTGGAACCCCCTCT
SLC46A3 sgRNA 1	CAAACAGAGCCAAACGC
SLC46A3 sgRNA 2	AATGTAGACACTAGACC
MFSD12 sgRNA 1	AAGGACAGCAGGACGCAGA
MFSD12 sgRNA 2	GCCTCGTAGCCCACGAG
WDR81 sgRNA 1	ACCTGGAAAAAGGTGGCCA
WDR81 sgRNA 2	TGAACTGCTGCCGAGT
WDR91 sgRNA 1	TTAATGCAGGTGTATGACT
WDR91 sgRNA 2	GCCACGGAACTCCAGAACC
CTSA sgRNA 1	CTCTCCAGGAGGCGCCC
CTSA sgRNA 2	CATGACCAGCACGGCCA
RAB7A sgRNA 1	TTGCTGAAGGTTATCATCC
RAB7A sgRNA 2	CTGAAGGTTATCATCCT
RMC1 sgRNA 1	CAAGATCACGGCGCTCT
RMC1 sgRNA 2	CAAGATCACGGCGCTCT
CTNS sgRNA	GAAATCACTCCAATCAGAC
XPNPEP sgRNA 1	CAGCTCTGAAGTCACCTT
XPNPEP sgRNA 2	CCCGCCGACAGTCACA
GNE sgRNA 1	ACATGCCATAACAAAAC
GNE sgRNA 2	TTTAACTGCACGAAAGTT
CMAS sgRNA 1	CGGGGGTCCCGCTCAT
CMAS sgRNA 2	TGCTTAATGTTCTTCA
NANS sgRNA 1	AATACCCTATGGGAATGTC
NANS sgRNA 2	CACTGACCGCACCAGCT
control sgRNA 1	CTTATAGGCTGGATTAT
control sgRNA 2	GCTTGAAACCAAGTGCTA

Sequences of sgRNA transduced into HeLa cells for gene knock down	
Gene	**5' to 3' sequences**
RMC1 sgRNA 1	CGCCCGCCATGGGCGAGG
RMC1 sgRNA 2	CCGGCCCGGACTGTAGCGG
RAB7A sgRNA 1	CTGGGCCCGCTGCTTACCG
RAB7A sgRNA 2	GCCATAAAGCCTGAGGCGG
control sgRNA 1	CTTATAGGCTGGATTAT
control sgRNA 2	GCTTGAAACCAAGTGCTA

Supplementary Figure 1

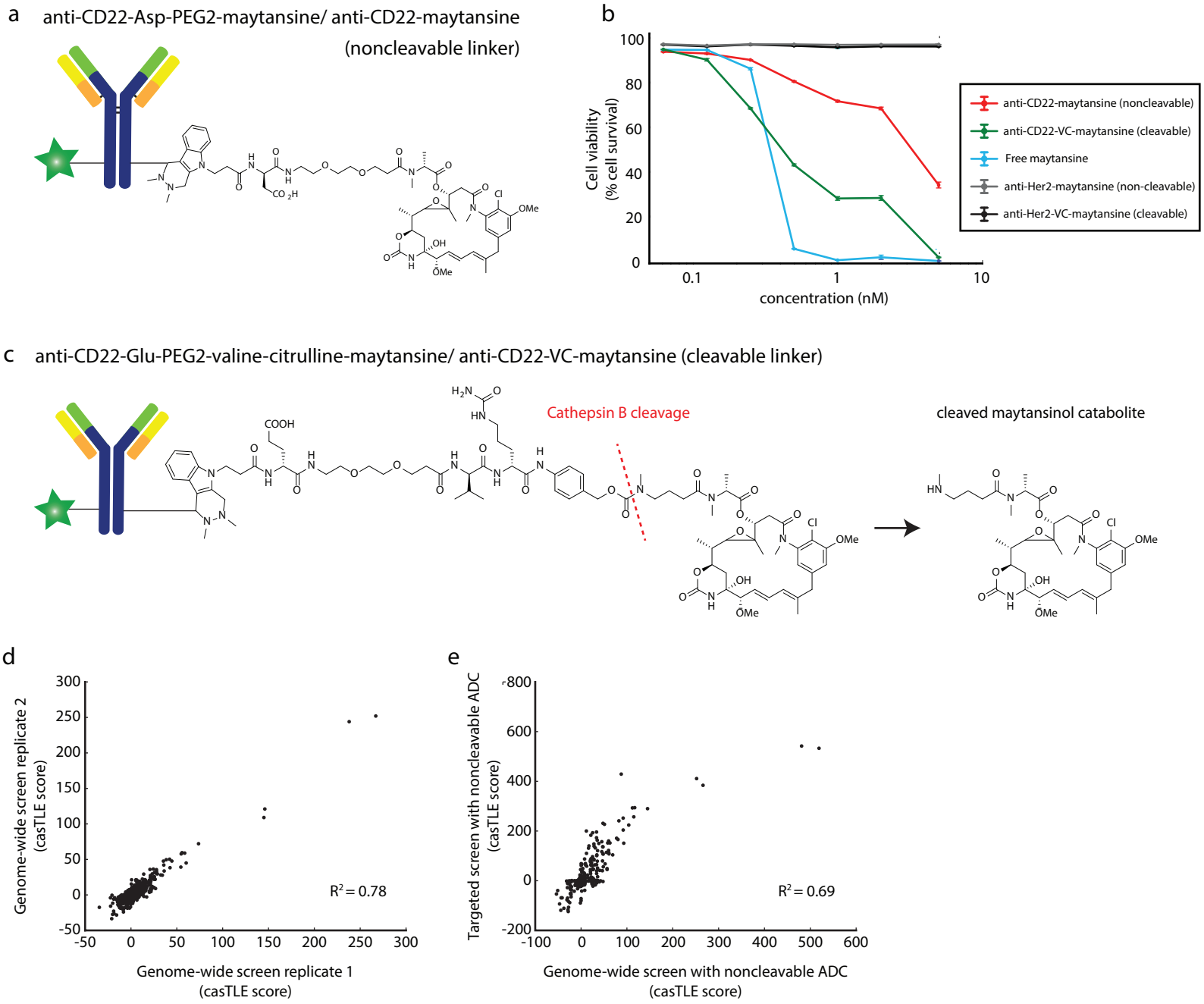

Supplementary Figure 1: ADC structures and their in vitro efficacy.

a. Linker and payload structure of anti-CD22-maytansine (noncleavable linker) ADC.

b. Cell viability of Ramos cells treated with indicated ADCs after 3 days. Viability was as determined by forward and side scatter live gating of Ramos cells (n=3; error bars, ± SEM)

c. Linker and payload structure of anti-CD22-VC-maytansine (cleavable linker) ADC. Also depicted is the predicted cathepsin B cleavage site and the resulting catabolite.

d. Replication plot of genome-wide screen in Fig. 1b. R-squared value is from a linear regression mode.

e. Replication plot of genome-wide screen and sublibrary screen using noncleavable linker anti-CD22 ADC. R-squared value is from a linear regression model.

Supplementary Figure 2

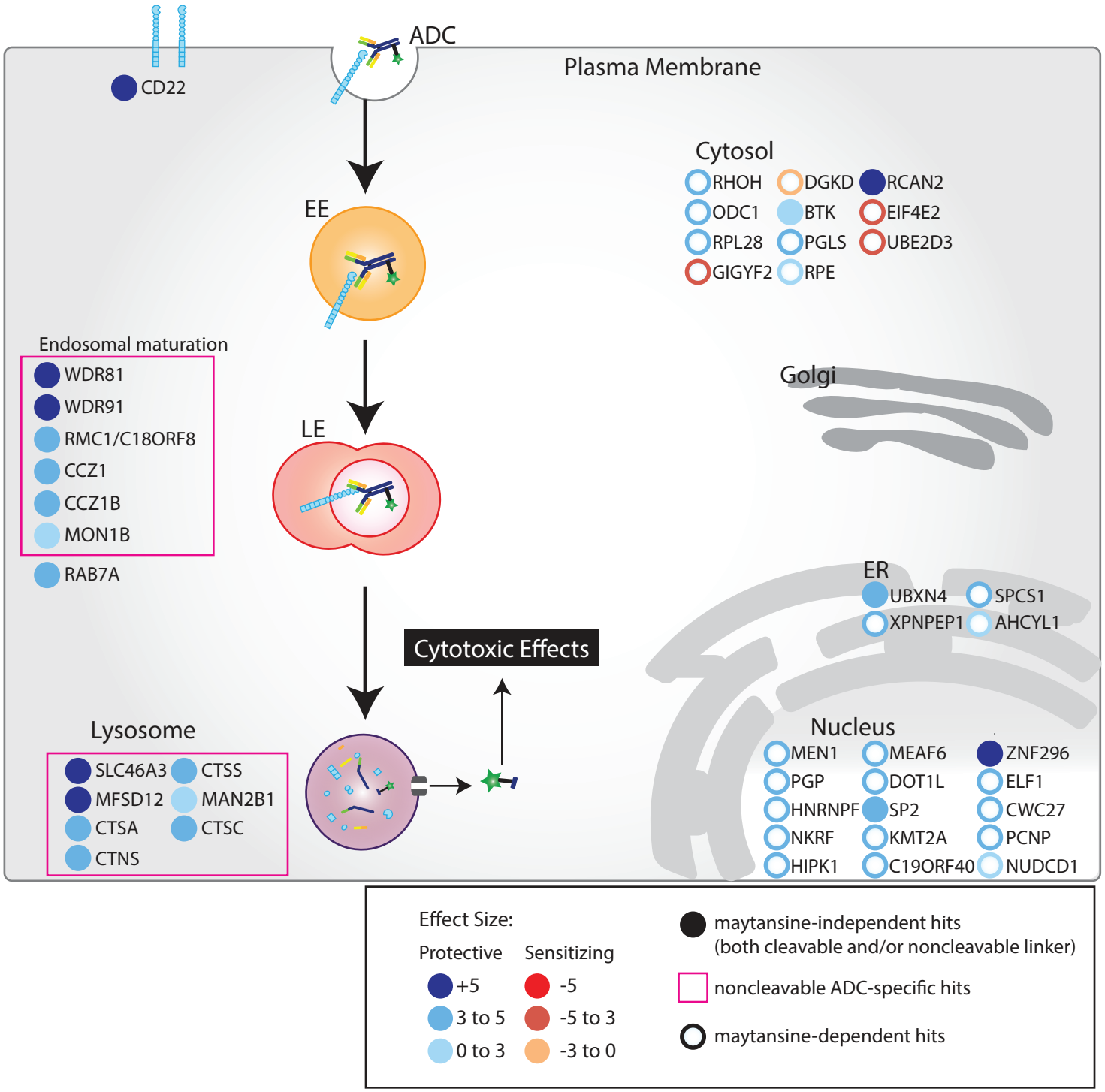

Supplementary Figure 2: Summary of screen hits from anti-CD22-maytansine (noncleavable), anti-CD22-VC maytansine (cleavable), and free maytansine.

Schematic for screen hits from anti-CD22-maytansine (noncleavable), anti-CD22-VC-maytansine (cleavable), and free maytansine. Depicted are the top 30 hits and selected endolysosomal genes, color coded by effect size (calculated by casTLE). Filled in circles represent maytansine-independent hits and empty circles represent maytansine-dependent hits. Hits unique to noncleavable linker ADC is denoted by pink box. Subcellular localization are indicated according to GO annotations.

Supplementary Figure 3

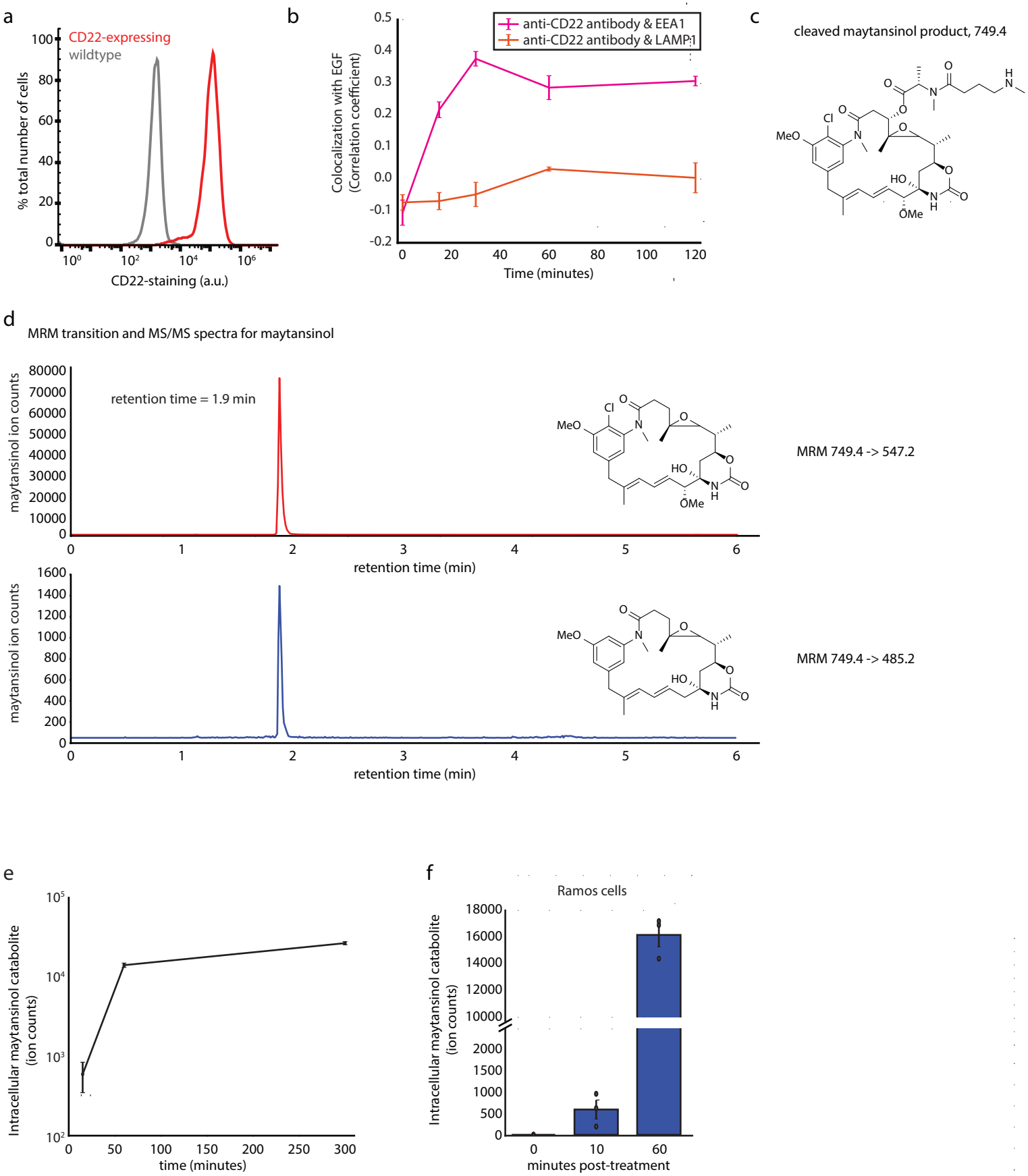

Supplementary Figure 3: Detection of ADC catabolite by LC/MS-MS.

a. Cell surface CD22-staining in HeLa cells stably expressing CD22, measured using anti-CD22-AF488 antibody followed by flow cytometry. Data are presented as mean ± SEM and are representative of two independent experiments performed in triplicate with consistent results.

b. Colocalization quantification for confocal microscopy images of anti-CD22 internalization in HeLa cells. Degree of colocalization of anti-CD22 antibody with early endosomal marker EEA1 and lysosomal marker LAMP1 is measured by Pearson's Correlation. Data are presented as mean ± SEM and are representative of two independent experiments performed in triplicate with consistent results..

c. Structure of cleaved maytansinol payload.

d. MRM transition and MS/MS spectra for maytansinol payload.

e. Maytansinol release from anti-CD22-VC-maytansine in CD22-expressing HeLa cells. Following anti-CD22-VC-maytansine addition, level of intracellular maytansinol catabolite was determined by LC/MS-MS at indicated time points; see methods for detailed extraction and detection protocols. Data are presented as mean ± SEM and are representative of three independent experiments performed in triplicate with consistent results.

f. Maytansinol release from anti-CD22-VC-maytansine in wild type Ramos cells. 10 nM anti-CD22-VC-maytansine was added to cells and reactions were quenched at indicated time points. Level of intracellular maytansinol catabolite was determined by LC/MS-MS; see methods for detailed extraction and detection protocol. Maytansinol signal is normalized by cell number and internal standard MMAE. Data are presented as mean ± SEM and are representative of three independent experiments performed in triplicate with consistent results.

Supplementary Figure 4

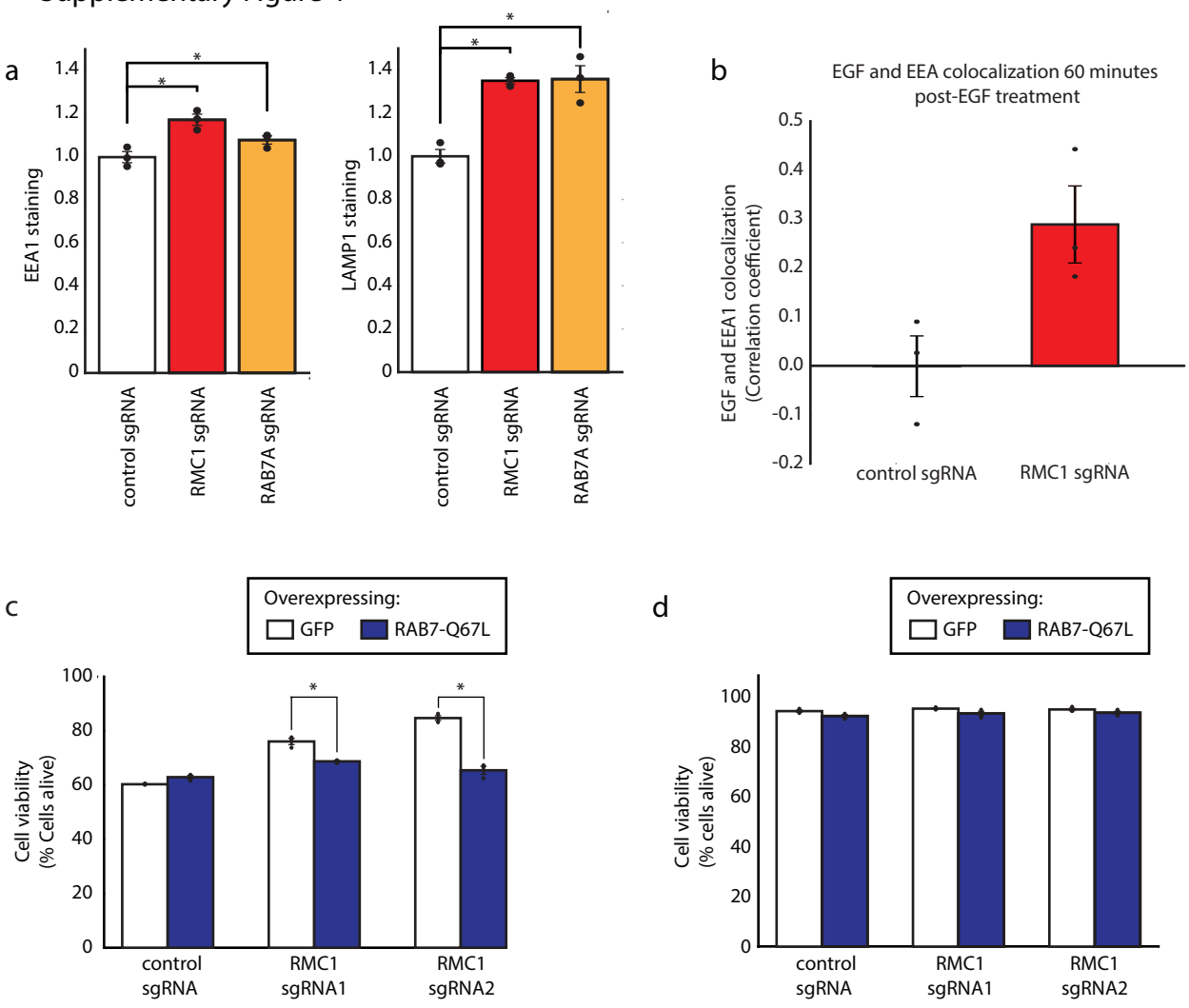

Supplementary Figure 4: Depletion of RMC1 alters endosomal and lysosomal morphology.

a. Total levels of EEA1 and LAMP1 in HeLa cells expressing the indicated CRISPRi sgRNA constructs. Cells were fixed, permeabilized, and stained with anti-EEA1 and anti-LAMP1 antibodies, followed by fluorescent secondary antibodies, and assayed by flow cytometry. normalized by cell number and internal standard MMAE. Data are presented as mean ± SEM and are representative of three independent experiments performed in triplicate with consistent results (Two-tailed t test, *P<0.05).

b. Colocalization quantification for confocal microscopy images of EGF trafficking in wild type and RMC1-knock down HeLa cells. Degree of colocalization of EGF and lysosomal marker LAMP1 is measured by Pearson's Correlation. Data are presented as mean ± SEM and are representative of two independent experiments performed in triplicate with consistent results.

c. Overexpression of constitutively active RAB7A-Q67L restores sensitivity towards anti-CD22-maytansine (noncleavable) in RMC1-knockout Ramos cells. Cells were treated with 1 nM anti-CD22 noncleavable linker ADC and cell viability was analyzed after three days of ADC treatment by flow cytometry. Viability was as determined by forward and side scatter of live gating of Ramos cells. Data are presented as mean ± SEM and are representative of three independent experiments performed in triplicate with consistent results (Two-tailed t test, *P<0.05).

d. Viability of Ramos cells overexpressing constitutively active RAB7A-Q67L. Cells were left untreated for three days and their viability, determined by forward and side scatter live gating, was measure by flow cytometry.Data are presented as mean ± SEM and are representative of two independent experiments performed in triplicate with consistent results.

Supplementary Figure 5

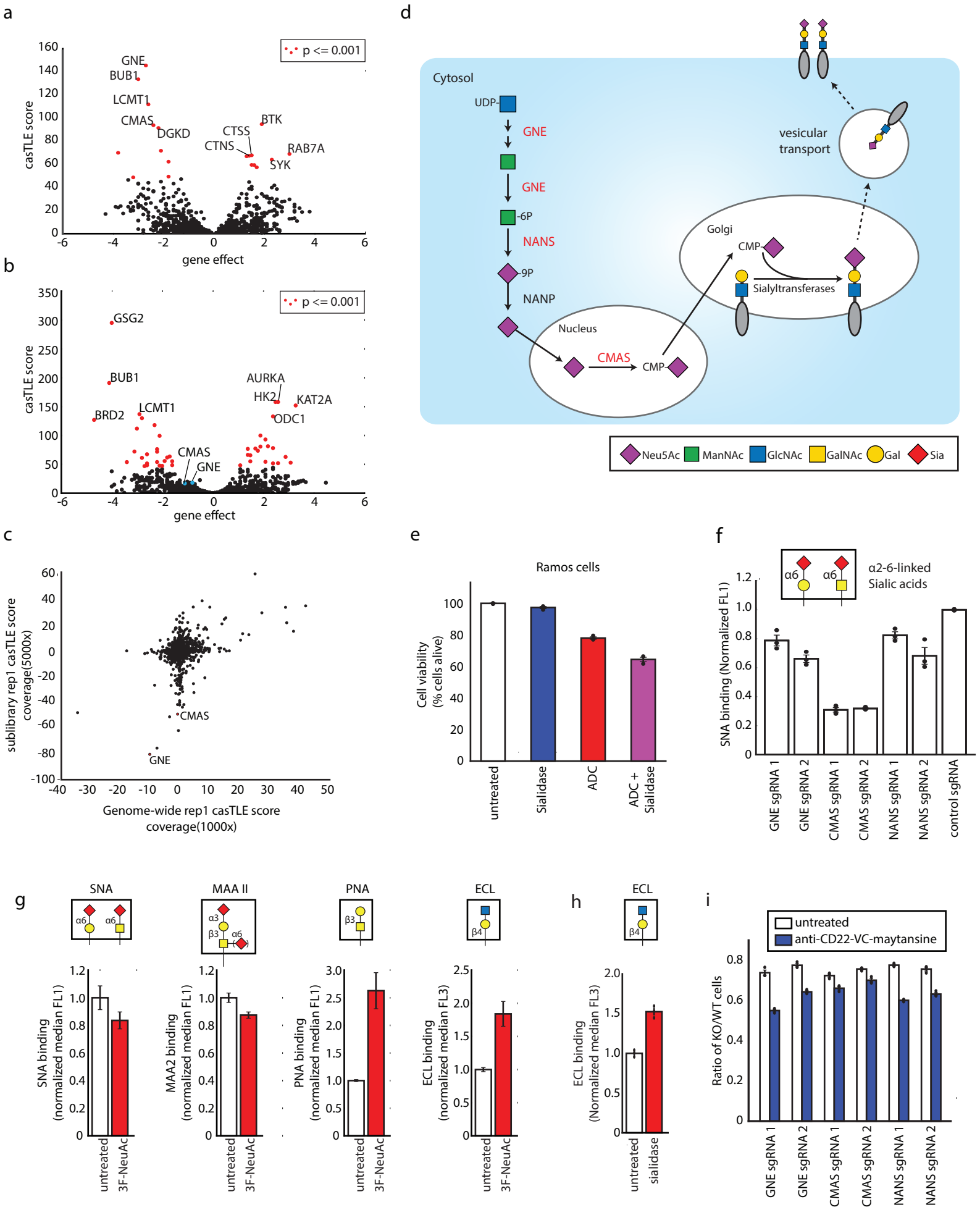

Supplementary Figure 5: Targeted screen uncovers role of sialic acid biosynthesis in regulation of ADC toxicity.

a. Volcano plot of all genes indicating effect and confidence scores for the drug target, kinases and phosphatases sublibrary anti-CD22-maytansine (noncleavable) screen. Effect and confidence scores determined by casTLE.

b. Volcano plot of all genes indicating effect and confidence scores for the drug target, kinases and phosphatases sublibrary free maytansine screen. Effect and confidence scores determined by casTLE. GNE and CMAS are not hits in the screen and are highlighted in blue.

c. Comparative analysis of results from genome-wide (1000x coverage, 2 nM anti-CD22-maytansine) and sublibrary (5000x coverage, 0.5 nM anti-CD22-maytansine) screens. Signed casTLE scores are reported.

d. Schematic for sialic acid synthesis pathway. Genes in red are validated using competitive assay shown in Fig. 5c.

e. Cell viability of Ramos cells treated with 25 nM Vibrio cholerae sialidase, anti-CD22-maytansine, or combination of both, assayed by flow cytometry. Viability was as determined by forward and side scatter of live gating of Ramos cells. Data are presented as mean ± SEM and are representative of three independent experiments performed in triplicate with consistent results.

f. Levels of α-2,6 sialic acid on KO Ramos cells as measured by labeling with SNA, a lectin that preferentially binds to α-2,6 sialic acid residues on N- and O-glycans (schematic illustrated in figure; red diamond: sialic acid/Sia, yellow square: N-acetylglucosamine/GalNAc, yellow circle: galactose/Gal). SNA conjugated to AF488 was incubated with cells on ice for 30 minutes. Cells were then washed 3x with cold PBS and analyzed by flow cytometry. Data are presented as mean ± SEM and are representative of two independent experiments performed in triplicate with consistent results.

g. Levels of cell surface sialic acid and "uncapped" glycans on Ramos cells treated with 12.5 μM 3F-NeuAc as detected by the indicated lectin. Ramos cells were treated with 3F-NeuAc for 48 hours, washed and stained by indicated lectins. The binding preferences of each lectin are depicted. Data are presented as mean ± SEM and are representative of two independent experiments performed in triplicate with consistent results.

h. Levels of "uncapped" glycans on Ramos cells treated with 25 nM Vibrio cholerae sialidase as detected by Erythrina cristagalli lectin (ECL). Ramos cells were treated with 25 nM Vibrio cholerae sialidase for one hour in PBS, washed and stained by ECL. Data are presented as mean ± SEM and are representative of two independent experiments performed in triplicate with consistent results.

i. Competitive growth assays in Ramos cells using VC cleavable linker ADC. Cells expressing sgRNAs for KO of indicated genes (mCherry+) and control (mCherry-) were co-cultured in 1:1 ratio. Cells were either treated with anti-CD22-VC-maytansine or left untreated for three days. Resulting ratio of KO:control was determined using flow cytometry. Data are presented as mean ± SEM and are representative of two independent experiments performed in triplicate with consistent results.

Supplementary Figure 6

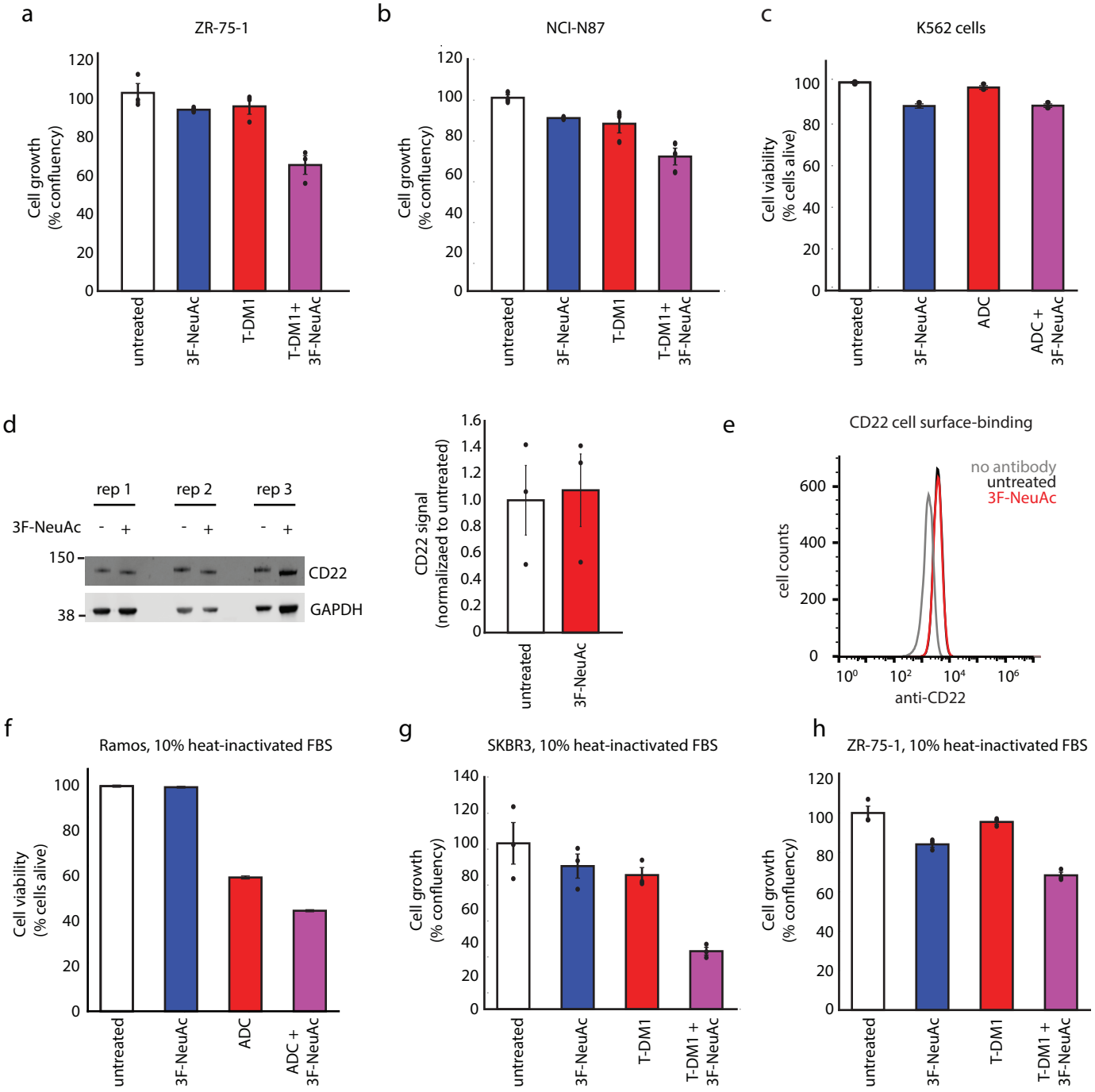

Supplementary Figure 6: Increased sensitivity to ADC by inhibiting sialylation is not due to alteration of CD22 cell surface levels or enhanced complement-mediated cell killing

a & b. Cell growth (% normalized confluency) of ZR-75-1 (a) and NCI-N87 (b) treated with 3F-NeuAc, T-DM1, or combination of both. Cells were pre-treated with 100 μM 3F-NeuAc for 48 hours, followed by incubation with 2 nM T-DM1. Confluency was determined by IncuCyte s3 Live cells analysis system and normalized to maximum confluency of the untreated condition at the end of the 5-day experiment. Data are presented as mean ± SEM and are representative of two independent experiments performed in triplicate with consistent results.

c. Cell viability of CD22-negative K562 cells treated with 100 μM 3F-NeuAc, 10 nM anti-CD22-maytansine, or combination of both, assayed by flow cytometry. Viability was as determined by forward and side scatter of live gating of K562 cells. Data are presented as mean ± SEM and are representative of two independent experiments performed in triplicate with consistent results.

d. CD22 whole cell protein levels measured by Western blot in Ramos cells. Cells were treated with 12.5 μM 3F-NeuAc for 48 hours, washed, and lysed for protein extraction. Western blotting was used to detect levels of CD22. Data are presented as mean ± SEM and are representative of two independent experiments performed in triplicate with consistent results. Please see Supplementary Fig. 8 for uncropped Western blot.

e. CD22 cell surface staining measured by flow cytometry in Ramos cells. Cells were treated with 12.5 μM 3F-NeuAc for 48 hours, washed, stained with AF488-labeled anti-CD22 antibodies, and analyzed by flow cytometry. Data are presented as mean ± SEM and are representative of three independent experiments performed in triplicate with consistent results.

f. Cell viability of Ramos cells treated with 3F-NeuAc, anti-CD22-maytansine, or combination of both in media supplemented with heat-inactivated fetal bovine serum, assayed by flow cytometry. Viability was as determined by forward and side scatter of live gating of Ramos cells. Data are presented as mean ± SEM and are representative of two independent experiments performed in triplicate with consistent results.

g & h. Cell growth (% normalized confluency) of SKBR3 (g) and ZR-75-1 (h) treated with 3F-NeuAc, T-DM1, or combination of both, in media supplemented with heat-inactivated fetal bovine serum. Cells were pre-treated with 100 μM 3F-NeuAc for 48 hours, followed by incubation with 2 nM T-DM1. Confluency was determined by IncuCyte s3 Live cells analysis system and normalized to maximum confluency of the untreated condition at the end of the 5-day experiment. Data are presented as mean ± SEM and are representative of two independent experiments performed in triplicate with consistent results.

Supplementary Figure 7

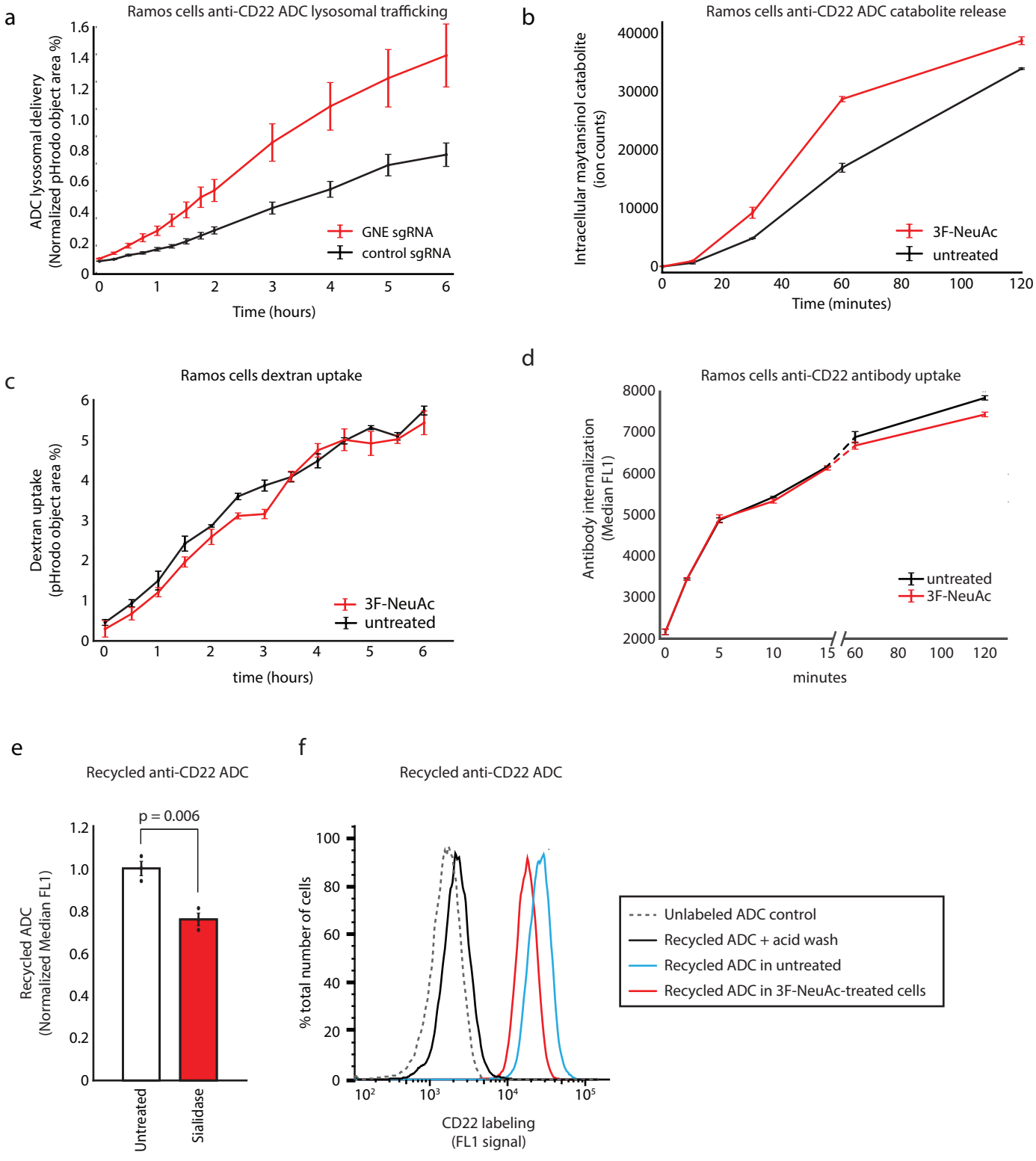

Supplementary Figure 7: Depletion of sialic acids reduces ADC recycling rates

a. Internalization of pHrodo-labeled anti-CD22 ADC in Cas9-expressing Ramos cells with either GNE sgRNA (red) or control sgRNA (black). pHrodo signal was measured using IncuCyte s3 Live cells analysis system and normalized to cell area. Data are presented as mean ± SEM and are representative of three independent experiments performed in triplicate with consistent results.

b. Maytansinol payload release in 3F-NeuAc-treated Ramos cells. Cells were pre-treated with 3F-NeuAc 12.5 μM for 48 hours, followed by incubation with anti-CD22-VC-maytansine for indicated times. Level of intracellular maytansinol catabolite was determined by LC/MS-MS; see methods for detailed extraction and detection protocol. Maytansinol signal is normalized by cell number and internal standard MMAE. Data are presented as mean ± SEM and are representative of three independent experiments performed in triplicate with consistent results.

c. Internalization of pHrodo-labeled dextran in Ramos cells. pHrodo signal was measured using IncuCyte s3 Live cells analysis system and normalized to cell area. Data are presented as mean ± SEM and are representative of three independent experiments performed in triplicate with consistent results.

d. Internalization of Alexa Fluor 488-labeled anti-CD22 antibody in wildtype Ramos cells either treated with 3F-NeuAc (red) or left untreated (black). Cells were incubated on ice with 10 μg/ mL labeled antibody for 20 minutes, followed by addition of 10X volume of pre-warmed media to initiate internalization. At indicated time points, cells were washed 2x with cold dPBS and washed once with acid wash to remove surface-bound antibodies. Intracellular levels of fluorescent antibodies were measured by flow cytometry. Data are presented as mean ± SEM and are representative of three independent experiments performed in triplicate with consistent results.

e. Recycling of anti-CD22 ADCs in Ramos cells pre-treated with 25 nM Vibrio cholerae sialidase for one hour (red) or left untreated (white). Cells were treated with unlabeled anti-CD22 ADC for an hour, acid-washed to remove surface-bound ADCs, and returned to 37°C for 30 minutes to allow for ADC recycling. ADCs recycled back to the cell surface are detected by Alexa Fluor 488-labeled anti-human IgG antibodies and analyzed using flow cytometry. Data are presented as mean ± SEM and are representative of two independent experiments performed in triplicate with consistent results.

f. Example of flow cytometry analysis in ADC recycling assay. Ramos cells that underwent ADC uptake and recycling (from Fig. 6c and Supplementary Fig. 7e) are stained with anti-human IgG antibodies conjugated to Alexa Fluor 488 (red line: 3F-NeuAc-treated cells, blue line: untreated control cells). As controls, cells treated only with unlabeled ADC (grey dotted line) and cells subjected to a second acid-wash step after recycling prior to staining with anti-human IgG-Alexa Fluor 488 (black line) are shown.

Supplementary Figure 8

Uncropped Western blots

Fig. 4d

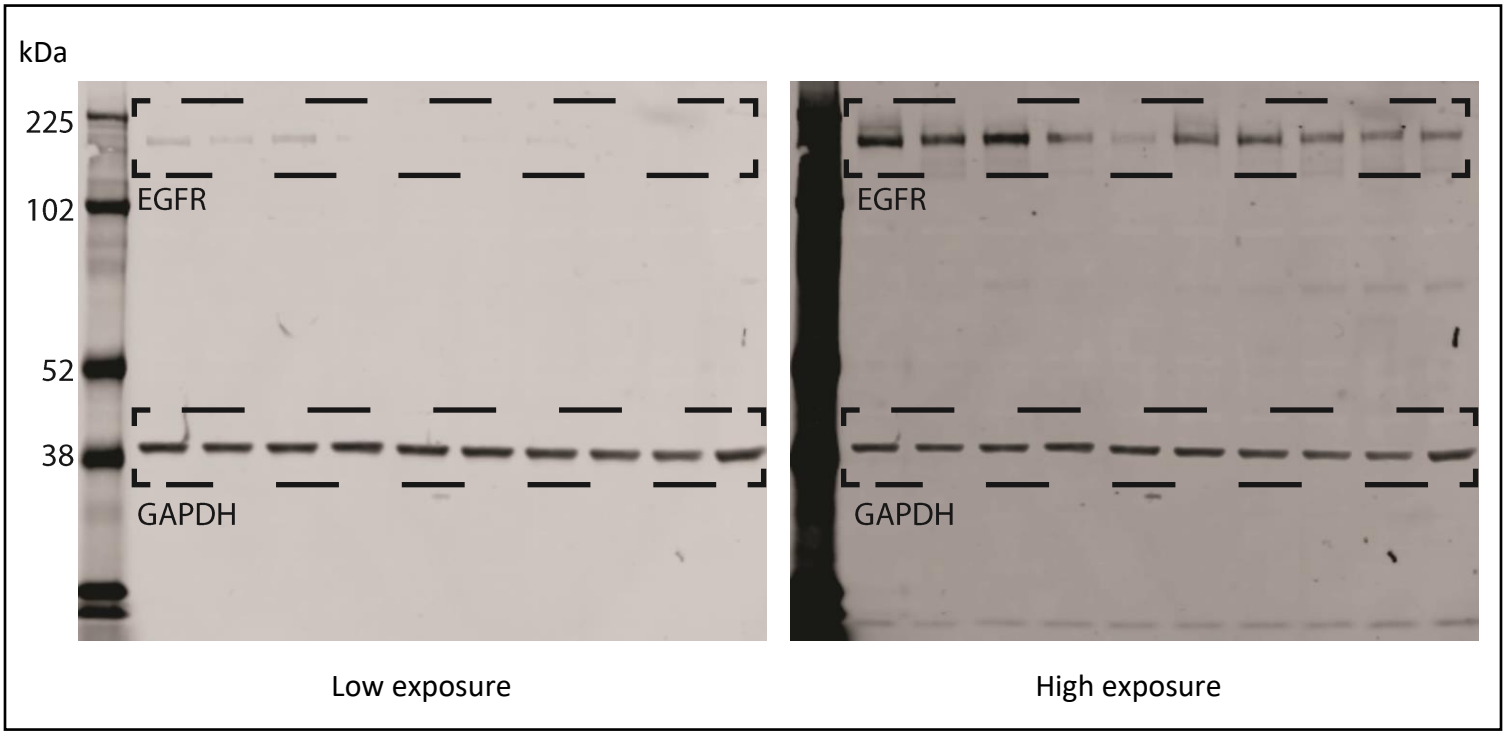

Supplementary Fig. 6d

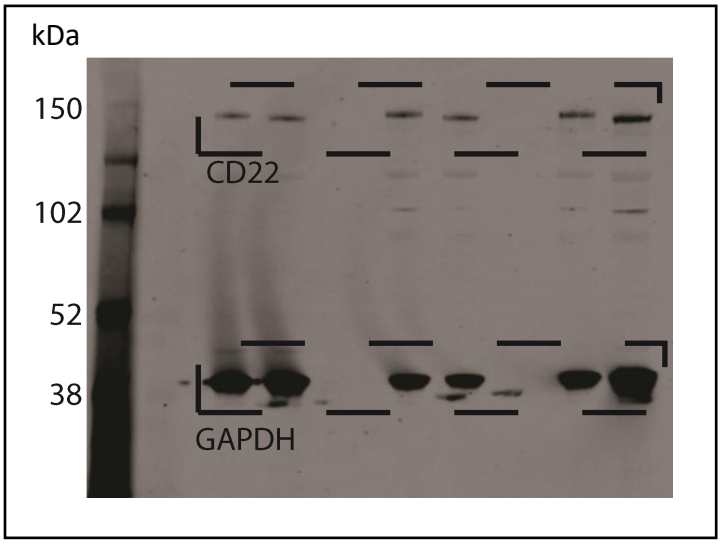

Supplementary Dataset Legends

Supplementary Dataset 1: Genome-wide CRISPR screen results with anti-CD22-maytansine ADC in Ramos cells.

Supplementary Dataset 2: ADC/endolysosomal sublibrary screen results with anti-CD22-maytansine (noncleavable ADC), anti-CD22-VC-maytansine (cleavable ADC), and free maytansine in Ramos cells.

Supplementary Dataset 3: Drug target, kinases, and phosphatases sublibrary screen results with anti-CD22-maytansine (noncleavable ADC) and free maytansine in Ramos cells.

Supplementary Dataset 4: Count files for all screens in Ramos cells.

Supplementary Dataset 5: ADC/endolysosomal sublibrary sgRNA composition.